Kerry A. Danelson
Department of Orthopaedic Surgery,
Wake Forest University Health Sciences,
Wake Forest University School of Medicine,
Medical Center Boulevard,
Winston-Salem, NC 27157;
Virginia Tech - Wake Forest University School of
Biomedical Engineering
and Sciences,
Blacksburg, VA 24061
e-mail: kdanelso@wakehealth.edu

Adam J. Golman
School of Biomedical Engineering
and Sciences,
Wake Forest University School of Medicine,
Suite 120, 575 N. Patterson Avenue,
Winston-Salem, NC 27101;
Virginia Tech - Wake Forest University School of
Biomedical Engineering and Sciences,
Blacksburg, VA 24061
e-mail: adam.golman@gmail.com

John H. Bolte IV
The Ohio State University,
Room #279,
1645 Neil Avenue,
Columbus, OH 43210
e-mail: bolte.6@osu.edu

Joel D. Stitzel[1]
School of Biomedical Engineering and Sciences,
Wake Forest University School of Medicine,
Suite 120, 575 N. Patterson Avenue,
Winston-Salem, NC 27101;
Virginia Tech - Wake Forest University School
of Biomedical Engineering
and Sciences,
Blacksburg, VA 24061
e-mail: jstitzel@wakehealth.edu

Simulation of Occupant Response in Space Capsule Landing Configurations With Suit Hardware

The purpose of this study was to compare the response of the total human model for safety (THUMS) human body finite element model (FEM) to experimental postmortem human subject (PMHS) test results and evaluate possible injuries caused by suit ring elements. Experimental testing evaluated the PMHS response in frontal, rear, side, falling, and spinal impacts. The THUMS was seated in a rigid seat that mirrored the sled buck used in the experimental testing. The model was then fitted with experimental combinations of neck, shoulder, humerus and thigh rings with a five-point restraint system. Experimental seat acceleration data was used as the input for the simulations. The simulation results were analyzed and compared to PMHS measurements to evaluate the response of the THUMS in these loading conditions. The metrics selected to compare the THUMS simulation to PMHS tests were the chest acceleration, seat acceleration and belt forces with additional metrics implemented in THUMS. The chest acceleration of the simulations and the experimental data was closely matched except in the Z-axis (superior/inferior) loading scenarios based on signal analysis. The belt force data of the model better correlated to the experimental results in loading scenarios where the THUMS interacted primarily with the restraint system compared to load cases where the primary interaction was between the seat and the occupant (rear, spinal and lateral impacts). The simulation output demonstrated low injury metric values for the occupant in these loading conditions. In the experimental testing, rib fractures were recorded for the frontal and left lateral impact scenarios. Fractures were not seen in the simulations, most likely due to variations between the simulation and the PMHS initial configuration. The placement of the rings on the THUMS was optimal with symmetric placement about the centerline of the model. The experimental placement of the rings had more experimental variation. Even with this discrepancy, the THUMS can still be considered a valuable predictive tool for occupant injury because it can compare results across many simulations. The THUMS also has the ability to assess a wider variety of other injury information, compared to anthropomorphic test devices (ATDs), that can be used to compare simulation results.
[DOI: 10.1115/1.4028816]

Keywords: computer modeling, human body modeling, injury metrics

Introduction

During NASA's development of the new spacecraft for the Constellation project, the astronaut suits were also redesigned to be more modular and worn in a variety of environments [1]. To facilitate that design, rigid suit elements were placed on the neck, shoulders, arms, and legs to allow for quick disconnects [2]. The effect of these rigid elements on the body during landing was unknown; therefore, PMHS testing was conducted to evaluate astronaut risk of injury in simulated landing scenarios [1]. The purpose of this study was to supplement the analysis from PMHS tests with a human body human FEM to further evaluate the injury potential during these landing scenarios.

Existing FEMs. Human body FEMs have been used extensively to simulate motor vehicle crash (MVC) impacts and evaluate injury mechanisms and risks [3–5]. The current study used the THUMS version 1.61c. This model was developed for use in automotive testing and has been extensively validated against PMHS data [6,7]. In previous evaluations of the ORION crew module, THUMS was also used to compare simulation results with different suit to capsule attachment hardware placements [8]. An advantage of the THUMS, compared to other surrogates, was that the injury risk assessment capabilities were not limited by instrumentation placement. Therefore, the user can examine any region of interest for possible injury sources.

Chest acceleration and seat belt loads were selected to compare the results of the THUMS simulations to the data collected during the PMHS tests. After the comparable responses of the two models were compared, the THUMS simulations were compared to each other using additional injury metrics for the thorax and upper extremity to evaluate relative injury to the occupant from the ring configurations. The metrics selected to assess thorax injury were chest deflection, sternal deflection, chest viscous criterion, chest acceleration, the combined thoracic index, and chest acceleration—3 ms clip. These metrics have commonly been used to assess risk of occupant injury in MVCs [9]. To evaluate upper extremity injury, the moments in the humeri and clavicles were extracted from the simulation results. Additionally, the strain values were analyzed for the clavicles, humeri and ribs. The strain and moment values were compared to corresponding experimental values for fracture in the literature [10,11].

[1]Corresponding author.

Manuscript received October 11, 2013; final manuscript received September 12, 2014; published online January 29, 2015. Assoc. Editor: Brian D. Stemper.

Table 1 Experimental instrumentation

Location	Instrumentation	Measures
Seat back	Load cell	*X*,*Y*,*Z* forces
Seat back	Accelerometer	*X*,*Y*,*Z* accelerations
Seat pan	Load cell	*X*,*Y*,*Z* forces
Seat pan	Accelerometer	*X*,*Y*,*Z* accelerations
Harness	Load cell	*X*,*Y*,*Z* forces
Clavicle	Strain gages	Medial and lateral strain on the left and right
Humerus	Strain gages	Proximal and distal strain on the left and right
Scapula	Strain gages	Acromion strain on the left and right
Scapula	Strain gages	Scapula strain at the left and right inferior angle
Ribs	Strain gages	Strain on ribs 3–8 in the left and right sides
Sternum	Motion block	Linear and angular acceleration in *X*,*Y*,*Z*
T-8	Motion block	Linear and angular acceleration in *X*,*Y*,*Z*

Methods

Model Configuration. The occupant FEM used in this analysis was THUMS version 1.61c (Toyota Technical Development Corporation, Nagoya, Japan) which was modified to stabilize the model response in Z-loading configurations. The modifications adjusted response curves for the pelvis flesh, abdominal organ tissue and lung tissue that allowed for element stiffening under large compressions. The original pelvis flesh material was modeled as viscoelastic. In the current simulations, it was modified to a rubber model that used a stress versus strain curve as input. The new input curve included stiffening following 85% strain. The abdominal organ tissue had the elastic modulus stiffened from 38.4 MPa to 55 MPa. The lung tissue material model was changed from low density foam to a linear elastic material with an elastic modulus of 1.66 MPa. Additionally, all element failure criteria were removed to assess loading values in all the elements for the entire simulation. All simulations were conducted on a Linux cluster computer in LS-DYNA version 971 (LSTC, Livermore, California) with a time step of 6.67×10^{-7} s.

The simulations were developed to mirror the experimental test conditions described by McFarland [1]. In these experiments, PMHS were placed in different orientations (Table 1) on a hydraulically controlled gas energized sled with a rigid seat configuration. A space suit analog was developed that placed ring hardware at different locations on the subject to assess injury under these components. The subject was restrained with a five-point harness. Measurements taken during the experiment included accelerations, seat belt loads, and strains on the bone with instrumentation details listed in Table 1. There are no kinematic data from the tests available at this time.

The simulated seat configuration used was the same seat configuration as the experimental tests with rigid plates and a rigid head rest (Fig. 1). During the testing, the head was occasionally padded with foam of an unknown dimension and density. This foam was not modeled and head accelerations were not considered because of this discrepancy. The head rest was in different locations based on the direction of gravity in the model. In cases where the THUMS was sitting upright (*Z*-axis gravity), the head rest was midway between the seatback and the THUMS head. In the cases where THUMS was on its back (*X*-axis gravity) the headrest was flush with the seatback. The remainder of the seat was also modeled with a rigid material. A foot rest was included in all simulations. In the rear simulation a panel between the foot rest and the seat was constructed. The feet and arms were unrestrained or tied to the footrest or other arm, depending on the testing configuration. For the lateral testing conditions, a head, shoulder, arm, hip and thigh restraint were also added to the model.

Rings that were the same dimension as possible suit components were added to the PMHS testing configuration. In the simulations, these rings were modeled as rigid bodies and were placed on the THUMS in a multiple step process. First, the arms were rotated about a point on the scapula until they were parallel to the seat bottom. Next, the shoulder and arm rings were placed in the approximate initial position without initial penetration of the thorax flesh by the rings. To achieve the proper flesh deformation, a simulation was conducted to move the arms down by rotating the arm bones about the scapula point until they were at the side of the body. The pulse simulations started with this final ring configuration. The PMHS restraint system was a five-point racing harness with 7.62 cm (3 in.) straps with the belt angles measured on the pretest pictures of the seated PMHS using Image-J (NIH, Bethesda, MA).

There were several occupant configurations based on the direction of testing. The restraint condition and the rings modeled were dependent on the test orientation and are listed in the test matrix (Table 2). The impact description from this table will be used throughout the text to describe the load case being discussed (Fig. 1). For *X*-axis configurations (anterior/posterior loading) gravity acted along the *Z*-axis (superior to inferior). For all *Z*-axis (superior/inferior loading) and *Y*-axis (left/right loading) accelerations, the testing was conducted with gravity acting along the *X*-axis (anterior to posterior). For both gravity configurations, the model was settled in the seat with gravity prior to conducting simulations. For the cases with gravity acting along the negative *Z*-axis, 1 g was used to settle the model. For the other gravity direction, a 5 g body load was required to force the head back onto the headrest. These settled occupants did not have additional deformation of other body regions when compared to the configurations settled with 1 g. Additionally, this larger body load was only used in settling simulations with all simulations of the experimental conditions conducted using the correct 1 g body load. All PMHS ring tests were modeled with the directions and specific test configurations from the experimental configurations (Table 2).

Accelerations. The inputs for the THUMS simulations were the experimental accelerations of the seat applied directly to the modeled seat. The experimental seat accelerations were processed by filtering, zeroing and truncating the pulse. All filtering was conducting using CFC 600 [12]. After the data was filtered, the data was zeroed by averaging the first 10 ms of data then subtracting the average from the remainder of the data. Starting at 10 ms into the pulse, the data was traced backward until the first time the acceleration crossed the *x*-axis (the point where acceleration equaled zero). This time point was taken as the time zero for the

Table 2 Test matrix for PMHS simulations

Name	Impact	Seat direction	Gravity direction	Rings	Hand/foot restraint	Fig. 1 letter
81111	Rear	−X	−Z	Shoulder	No/no	*a*
81112	Frontal	+X	−Z	Shoulder	No/no	*b*
81113-1	Falling	−Z	+X	Shoulder	No/yes	*c*
81113-2	Spinal	+Z	+X	Thigh	Yes/yes	*d*
90421	Frontal	+X	−Z	Shoulder	Yes/yes	*b*
90422-3	Right lateral	−Y	+X	Shoulder + thigh	Yes/yes	*e*
90422-6	Left lateral	+Y	+X	Shoulder + thigh	Yes/yes	*f*

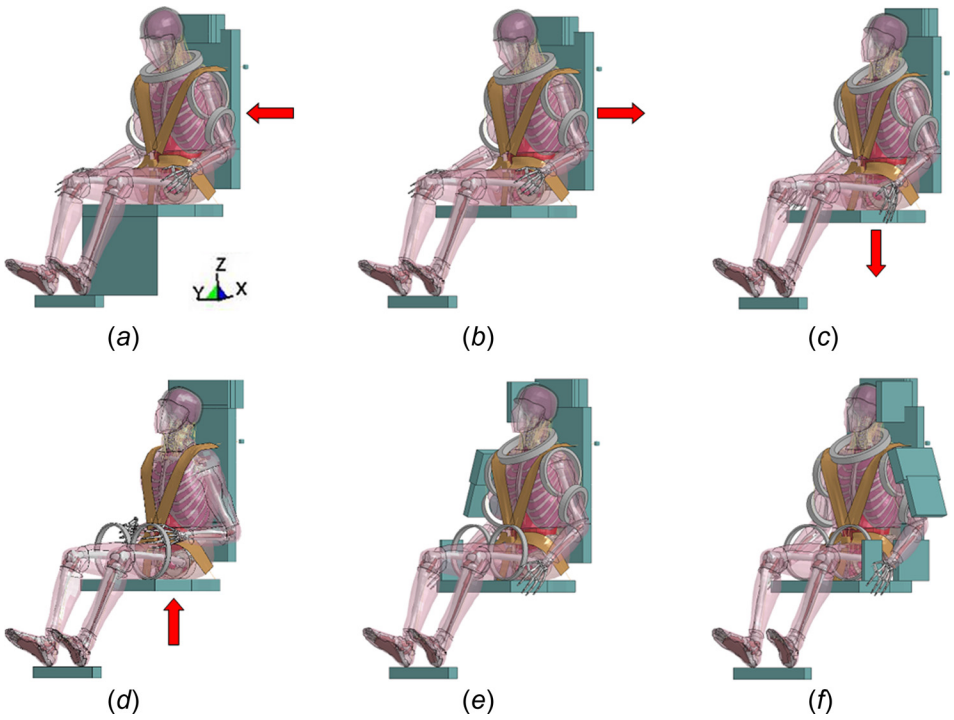

Fig. 1 THUMS seating configurations for testing with different ring configurations for different test conditions. Impact types are rear, posterior to anterior (*a*); frontal, anterior to posterior (*b*); falling, superior to inferior (*c*); spinal, inferior to superior (*d*); right lateral, right to left and (*e*); left lateral, left to right (*f*).

simulation. Finally, the data was truncated to minimize the amount of time required to run the simulation. The end time of the simulation was 20 ms after the maximum velocity of the pulse.

Injury Metric Calculations. Several injury metrics were selected to evaluate the THUMS response in comparison to the PMHS tests and the potential for injury in various regions throughout the body. The regions of interest were the thorax, upper extremities and lower injuries because these areas had interaction points between the restraint system and the occupant. N_{ij} was not evaluated or compared because the PMHS was wearing a foam neck collar to prevent excessive head movement. The tension in all belts and the acceleration of the seat were extracted from the simulations and compared to the recorded data from the PMHS tests.

Chest Metrics. Several injury metrics were selected to evaluate the response of the chest. They included peak chest acceleration, sternal deflection, chest deflection, and Viscous Criterion (V · C). Chest acceleration was measured from a node located at the centroid of T6. This location was selected because it most closely matches the measurement location of chest acceleration in an ATD. Sternal deflection was the change in the distance from a node to node on the sternum to the ninth thoracic vertebra (Fig. 2(*a*)). The maximum deflection value was compared between simulations.

Another metric used to quantify the compression of the chest was the chest deflection metric. This metric measured the deflection of seven ribs along a line from the sternum to the spine. Each line was horizontal; therefore, the front node was not on the same rib as the rear node. These deflections were measured to assess the overall response of the thorax (Fig. 2(*b*)).

The Viscous Criterion (V · C) combines deflection with the rate of deflection to evaluate the risk of soft tissue injury. A value of 1 is the accepted value for human tolerance and it is equivalent to a 25% chance of severe injury, as classified in the abbreviated injury scale as a 4+ injury [13]. In these simulations, the V · C was calculated from the sternal deflection measurements.

Strain Metrics. Strain was extracted from key anatomical regions of interest to evaluate the relative injury potential between simulations and compare to the PMHS injuries. These regions included the right humerus, left humerus, right clavicle, left clavicle, right ribs, and left ribs. The maximum strain from each of these regions was calculated by finding the maximum strain element and then averaging the strains in the adjacent elements to mitigate large strain value spikes in single elements.

Clavicle and Humerus Load and Moment. The right and left clavicle and humerus bending moments were determined in each simulation to further assess risk of fracture. These metrics were determined using custom section planes defined for the THUMS

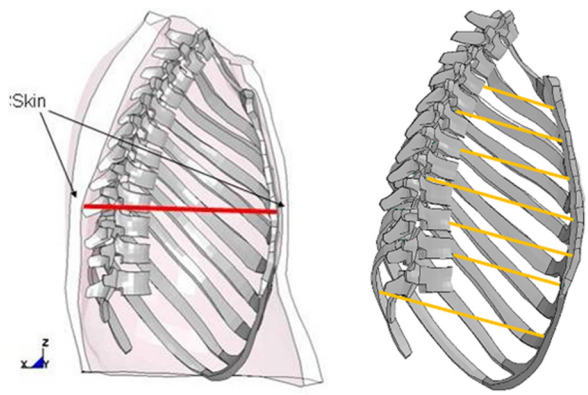

Fig. 2 The sternal (*a*, single line) and rib deflection (*b*, multiple lines) measurement locations for the THUMS simulations

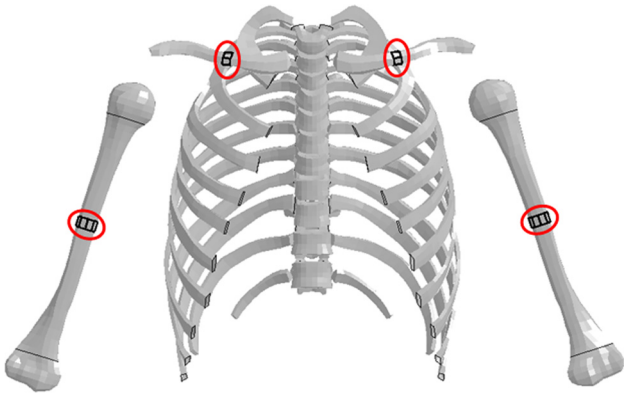

Fig. 3 Humerus and clavicle section plane locations

with section forces recorded for the simulation time history (Fig. 3). The resulting bending moment was compared to literature failure limits of 27.7 N · m [11] and 130–148 N · m [10] for the clavicle and humerus, respectively.

Comparison of the THUMS and the PMHS

PMHS Test Results. During the PMHS tests, extensive data from the test apparatus and the PMHS were collected [1]. To evaluate the response of the model, the simulation data were compared to the PMHS belt loads, chest acceleration, and injuries noted. The PMHS chest acceleration was measured at T8 or T4 (81113-1, 81113-2, 90422-3, and 90422-6). Table 3 contains basic subject data and the injuries noted during autopsy. As seen in this table, most of the test configurations did not result in injury to the occupant.

Comparison of the THUMS and PMHS. To compare the experimental and simulation results, two methods were used: a qualitative visual inspection of videos and quantitative signal comparisons. A qualitative visual assessment of the THUMS kinematics compared the d3plot files of the model and the PMHS test videos at the time of maximum engagement of the occupant with the restraint system. Maximum engagement was defined as the time when the occupant had fully loaded the belts or the seat structure and before rebound occurred. This time point coincided with maximum belt force. The next method for comparison was plotting the chest acceleration and belt forces for the experiments and simulations to quantify the similarities and differences in response. The metrics were selected because they were considered indicative of boundary conditions on the body. Given these matched plots, the signal similarity was compared using the method described by Sprague and Geers to quantify the variation between the magnitude and phase of two signals [14]. The signal comparison results calculated the difference in the signal magnitudes (M) and phase (P) using Eqs. (1)–(4). A perfect match of the signals would result in a value of 0 for each parameter. One parameter was not quantified, frontal case 81112 fifth point belt load, because there was missing experimental data.

$$\boldsymbol{M} = \sqrt{\frac{\vartheta_{\mathrm{mm}}}{\vartheta_{\mathrm{ee}}}} - 1 \text{ and } \boldsymbol{P} = \frac{1}{\pi}\arccos\left(\frac{\vartheta_{\mathrm{em}}}{\sqrt{\vartheta_{\mathrm{mm}}\vartheta_{\mathrm{ee}}}}\right) \tag{1}$$

where

$$\vartheta_{\mathrm{mm}} = \frac{1}{t_2 - t_1}\int_{t_1}^{t_2} \boldsymbol{m}^2(t)dt \tag{2}$$

$$\vartheta_{\mathrm{ee}} = \frac{1}{t_2 - t_1}\int_{t_1}^{t_2} \boldsymbol{e}^2(t)dt \tag{3}$$

$$\vartheta_{\mathrm{em}} = \frac{1}{t_2 - t_1}\int_{t_1}^{t_2} \boldsymbol{e}(t)\boldsymbol{m}(t)dt \tag{4}$$

In these equations, $m(t)$ and $e(t)$ correspond to the model and experimental signals, respectively. The magnitude and phase error factors are calculated over a time period from $t_1 \leq t \leq t_2$ where t_1 is time zero and t_2 is the end time.

Results

Qualitative Kinematic Results. A qualitative visual assessment of the THUMS response and the PMHS response from the experiment videos and simulation output demonstrated similarities between the gross motion of the THUMS and the PMHS (Appendix A). The primary difference noted between the THUMS and the PMHS results was additional arm excursion of the PMHS during the frontal tests.

THUMS Injury Metric Results

Chest. The chest acceleration values varied slightly between cases, except in the frontal impact 90421 which resulted in comparatively larger acceleration. In all cases, the remaining chest injury metrics had low values compared to established injury assessment reference values: sternal deflection = 6.3 cm and chest acceleration = 60 g [15]. The rear impact simulation had the highest sternal deflection, chest deflection and V · C (Table 4).

Clavicle and Humerus Analysis. For all cases the bending moments in the simulation were well below the fracture limits, 27.7 N · m for the clavicle and 130–148 N · m for the humerus (Table 5). In these simulations, frontal test 81112 had the highest clavicle and humerus loads. The spinal and lateral cases also had relatively high clavicle moments. The rear cases had the second highest humerus loads.

Strain Analysis. The highest strain elements were focused on the clavicle midshaft, humerus midshaft, superior ribs and inferior ribs. These locations corresponded to interaction with the seatback (lower posterior ribs), neck ring and restraints (high ribs), and shoulder rings (lateral inferior ribs). The frontal impact simulations had the highest strain values for most of the body regions of interest. None of the simulations had a maximum strain value that exceeded the fracture strain of 2.44% [16–18]. Fringe plots showing the strain locations are included in Appendix B and maximum strain values are shown in Tables 6 and 7.

Table 3 PMHS test subject anthropometry and injuries noted during autopsy

Test number	Age	Height (in. (cm))/weight (pounds (kg))	Injury
81111 (rear)	46	69.9 (177.5)/167 (75.5)	Scapula bruising
81112 (frontal)	56	68.5 (174.0)/181 (82.1)	Fractured ribs (left 2, 3, 4 and right 3, 4, 5)
81113-1 (falling)	74	69.3 (176.0)/175 (79.4)	No damage
81113-2 (spinal)	Same as 81113-2	Same as 81113-2	No Damage
90421 (Frontal)	60	69.0 (175.3)/161 (73.0)	Fractured ribs (left 3,4 and right 7)
90422-3 (right lateral)	71	67.3 (170.9)/194 (88.0)	No damage
90422-6 (left lateral)	Same as 90422-3	Same as 90422-3	Fractured ribs (Left 6, 7, 8

Table 4 Simulated chest injury metric results

Simulation	Sternal deflection (cm)	Rib deflection (cm)	Chest acceleration (g)	V · C (m/s)
81111 (rear)	−2.524	−1.517	18.82	−0.073
81112 (frontal)	−0.761	−0.320	23.71	−0.019
81113-1 (falling)	−0.788	−0.328	24.10	−0.020
81113-2 (spinal)	−1.036	−0.315	23.92	−0.039
90421 (frontal)	−0.322	−0.090	37.42	−0.006
90422-3 (right)	−0.188	−0.176	29.71	−0.003
90422-6 (left)	−0.188	−0.087	28.61	−0.001

Table 5 Simulated clavicle and humerus moments

Case	L clavicle (N · m)	R clavicle (N · m)	L humerus (N · m)	R humerus (N · m)
81111 (rear)	1.55	2.01	29.40	29.08
81112 (frontal)	8.92	7.35	41.54	51.82
81113-1 (falling)	4.54	4.34	18.41	17.12
81113-2 (spinal)	7.42	7.43	15.46	11.75
90421 (frontal)	6.45	6.32	38.90	37.86
90422-3 (right)	1.99	7.98	30.21	22.03
90422-6 (left)	7.34	1.40	24.23	24.94

THUMS to PMHS Comparison. In general, the THUMS and PMHS chest acceleration values were closely aligned (Table 8). Cases where the occupant interacted primarily with the seat structure had the most similar simulation chest acceleration compared to experimental values. Belt forces were generally well aligned in cases with occupant to belt interaction (frontal and falling cases). The other cases, with primary interaction between the seat and the occupant, had larger discrepancies between the compared belt forces.

Discussion

The gross THUMS motion compared well to the PMHS motion as seen in test videos with the primary difference between the two in extremity excursion (Appendix A). This similarity was expected because the THUMS was developed and validated using PMHS testing. A limitation of this observation is that it was a qualitative assessment of the test videos compared to the simulation output. Additional work needs to be done in the future to quantify the kinematics of the occupant through additional video analysis. The observed difference in response is most likely due to model configuration assumptions, such as the method of ring attachment. The discrete elements in the model used for ring attachments were stiffer than the belts used in testing. This difference results in a conservative model assessment because it places a higher load on the middle of the humerus in the simulations.

The quantitative signal analysis results demonstrated similar boundary conditions between the simulations and experimental testing. The largest differences were in measurements that had low values due to minimal occupant engagement, such as the shoulder belt loads in case 81111, which had the primary occupant engagement with the seat back.

In the PMHS testing, there were few injuries reported from autopsy. Similarly, the THUMS simulations predicted low injury metric values. It was hypothesized that the rib strain data would be the best correlate to PMHS injury. In the simulations, the maximum strains in the ribs were below the expected fracture limit of 2.44% strain. While the absolute strain value did not predict fracture, the relative strain data did demonstrate the same trends as the PMHS injury data. The simulations with highest rib strains (81112, frontal; 90421, frontal; and 90422-6, left) were all cases that had rib fracture in the PMHS. Additionally, the visual representations of the high strain areas also highlighted high strain elements on the ribs that fractured in experimental testing. In case 81112, the fractured ribs were left 2, 3, 4, and right 3, 4, 5. The corresponding THUMS strain measurements showed high strain in the superior ribs on 81112. In 90421, the fractured ribs were left 3, 4 and right 7. For 90421, there were high strains at the

Table 6 Maximum simulated rib and clavicle strain values for each case

Simulation number	Right ribs	Left ribs	Right clavicle	Left clavicle
811111	0.0029	0.0065	0.0022	0.0020
811112	0.0065	0.0074	0.0062	0.0065
90421	0.0097	0.0075	0.0048	0.0060
811113-1	0.0036	0.0060	0.0020	0.0024
811113-2	0.0056	0.0031	0.0056	0.0062
90422-3	0.0058	0.0033	0.0033	0.0014
90422-6	0.0060	0.0116	0.0011	0.0050
811111	0.0029	0.0065	0.0022	0.0020
811112	0.0065	0.0074	0.0062	0.0065

Table 7 Maximum simulated humerus strain values for each case

Simulation number	Right humerus	Left humerus
811111	0.0031	0.0034
811112	0.0041	0.0050
90421	0.0032	0.0037
811113-1	0.0025	0.0015
811113-2	0.0017	0.0019
90422-3	0.0018	0.0031
90422-6	0.0029	0.0028

Table 8 Quantitative signal comparison results where a value of 0 would indicate the same signal in magnitude (M) and phase (P). The two highest values are underlined and highlighted in red and the two lowest values are highlighted in green.

Sim. Number	Chest Acceleration		Left Shoulder Belt		Right Shoulder Belt		Left Lap Belt		Right Lap Belt		5th Point Belt	
	M	P	M	P	M	P	M	P	M	P	M	P
81111	-0.27	0.15	-0.43	0.25	-0.62	0.32	-0.61	0.13	-0.57	0.12	-0.75	0.29
81112	-0.43	0.23	0.21	0.11	0.04	0.11	0.35	0.10	0.17	0.12	None	None
81113-1	-0.45	0.27	0.06	0.12	0.05	0.11	-0.22	0.10	-0.29	0.10	0.09	0.12
81113-2	-0.27	0.11	-0.31	0.13	-0.40	0.12	-0.66	0.15	-0.68	0.20	-0.58	0.16
90421	-0.35	0.22	0.10	0.06	0.19	0.09	0.28	0.04	-0.06	0.09	0.20	0.09
90422-3	-0.35	0.22	-0.60	0.24	-0.75	0.22	-0.56	0.12	-0.67	0.22	-0.66	0.19
90422-6	-0.37	0.22	-0.77	0.24	-0.13	0.24	0.77	0.30	-0.52	0.17	-0.58	0.20

superior and lateral aspects of the ribs. The lateral cases were predicted to have relatively high humerus moments because of direct humerus loading. Instead, the placement of the lateral support structures had a protective effect because they were above the humerus rings and primarily interacted with the shoulder of the PMHS.

Overall, the experimental cases simulated did not result in a large number of injuries to the subjects. The simulation injury metrics used to analyze the THUMS results also did not indicate high injury metric values. Future work will investigate the source of the discrepancies between the simulations and experiments as well as simulate experiments with more injuries. However, this study was a first step in investigating the response of THUMS in a space capsule loading environment which had very different boundary conditions when compared to the automotive loading used in validating the model response.

Limitations. One limitation of this study is the relative lack of biomechanical data on bony failure properties of occupants exposed to long term zero-gravity. This exposure has the well documented effect of a reduction in bone mineral density [19]. The corresponding decrease in biomechanical strength would change the risk of injury in those occupants. However, much of the human tolerance data in biomechanical literature are derived from PMHS testing. Generally, the subjects used in these studies were older individuals with corresponding age related bone strength reduction. In this respect, the PMHS data is more like the returning crew members then the active and healthy crew members before launch.

Metric variation between the THUMS and the PMHS can be influenced by the slight differences in two configurations. The THUMS is the size of a 50th percentile male. The PMHS subjects were close but not the exact size as the THUMS; therefore, the exact location of the rings on the PMHS could not be replicated. Additionally, differences in occupant height and weight can change how and where the rings interact with the thorax. The THUMS ring placement was symmetrical about the center of the body. The PMHS test configurations had more experimental variation with the initial ring placement. Additionally, only the response of an average size male was assessed to be consistent with the experimental work; however, to fully assess suit response a range of occupant gender and size should be considered. Future work should investigate the effect of these variations on the overall response to determine model sensitivity to ring placement and occupant size.

Conclusions

The results of this comparison indicate the THUMS performed in a similar manner as the PMHS in these experimental tests. The gross movement of the model and the chest acceleration were well correlated for the majority of the simulations. The belt forces were not as similar between the PMHS and FEM for the tests with minimal belt engagement; however, tests with large belt engagement resulted in closer agreement between the measured values. The simulation rib strain measurements did not absolutely predict fracture but they demonstrated the same trends as the experimental tests. Therefore, the THUMS could be used as an effective comparison tool but not an absolute predictor of rib injury at this time.

Acknowledgment

Funding for this study was provided by NASA, Johnson Space Center. The authors would like to acknowledge the assistance of Nancy Currie, Ph.D., Antja Chambers, Dominick Mancuso, Brad Granderson, Jeff Somers, M.S., and the Orion Task 1 team. Computations were performed on the Wake Forest University DEAC Cluster, a centrally managed resource with support provided in part by the University. Eileen Martin provided the medical illustrations for this article.

Appendix A: Comparison of the THUMS and PMHS Kinematic Response From Simulation Output and Experimental Video

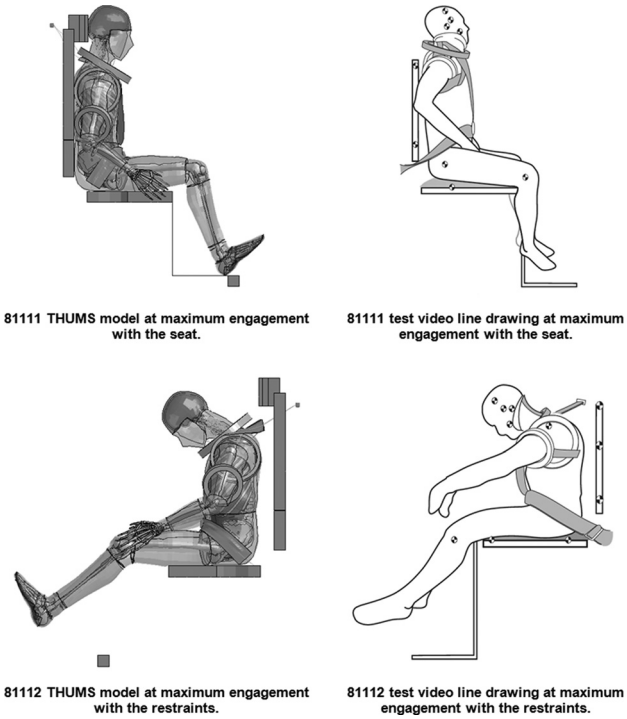

81111 THUMS model at maximum engagement with the seat.

81111 test video line drawing at maximum engagement with the seat.

81112 THUMS model at maximum engagement with the restraints.

81112 test video line drawing at maximum engagement with the restraints.

Fig. 4

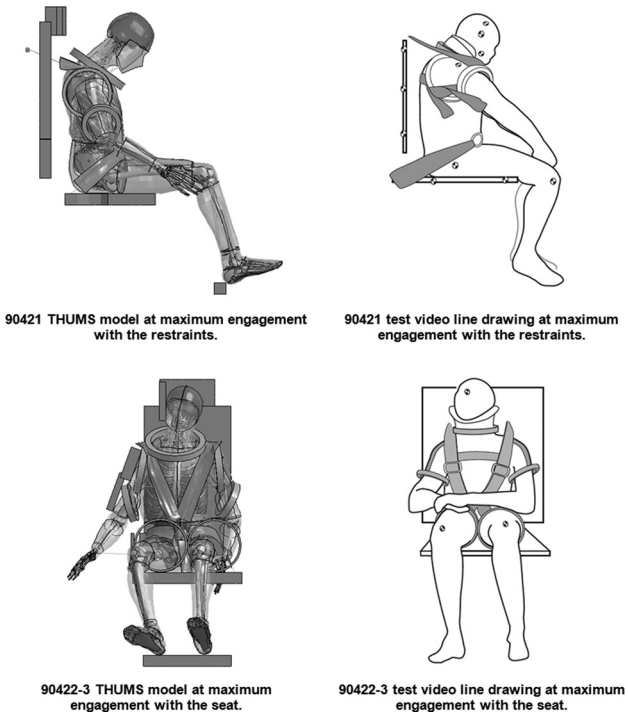

90421 THUMS model at maximum engagement with the restraints.

90421 test video line drawing at maximum engagement with the restraints.

90422-3 THUMS model at maximum engagement with the seat.

90422-3 test video line drawing at maximum engagement with the seat.

Fig. 6

Appendix B: Strain Assessment Results

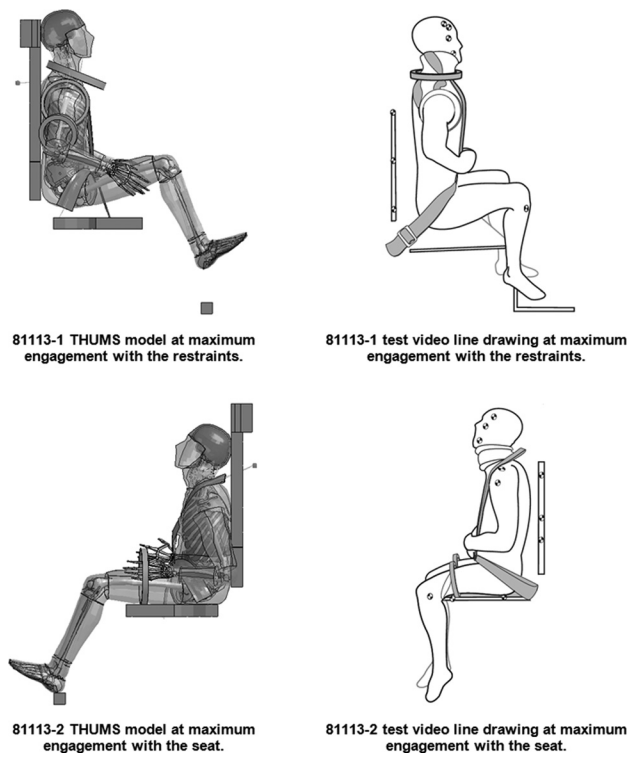

81113-1 THUMS model at maximum engagement with the restraints.

81113-1 test video line drawing at maximum engagement with the restraints.

81113-2 THUMS model at maximum engagement with the seat.

81113-2 test video line drawing at maximum engagement with the seat.

Fig. 5

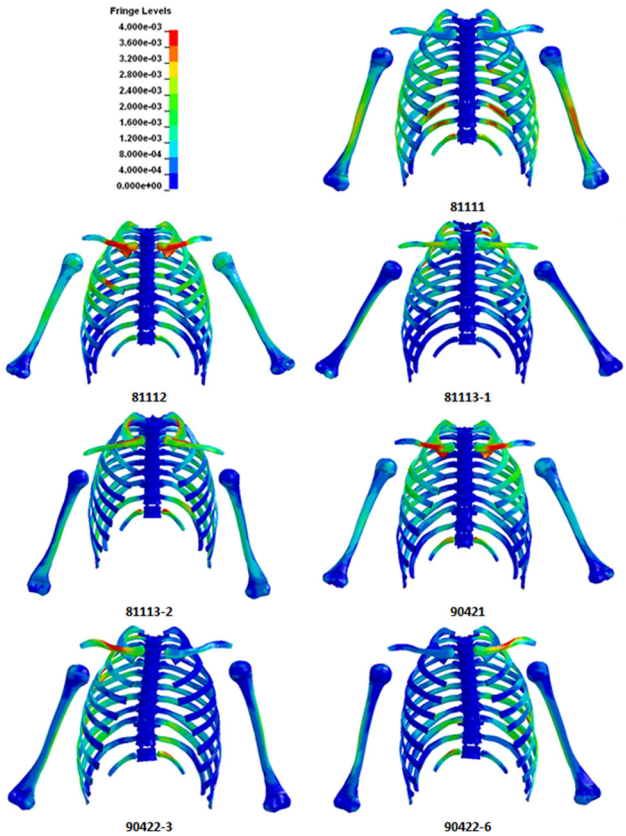

Fig. 7

References

[1] Mcfarland, S. M., 2011, "Testing Injury Potential of Suited Occupants During Dynamic Spacecraft Flight Phases," AIAA Paper No. 2011-5053, pp. 1–31.

[2] Ross, A., 2009, "Constellation Program Pressure Garment Development Activities," International Conference on Environmental Systems, Savannah, GA, SAE Technical Paper No. 2009-01-2553.

[3] Kitagawa, Y., Yasuki, T., and Hasegawa, J., 2006, "A Study of Cervical Spine Kinematics and Joint Capsule Strain in Rear Impacts Using a Human FE Model," Stapp Car Crash J., **50**, pp. 545–566.

[4] Siegel, J. H., Belwadi, A., Smith, J. A., Shah, C., and Yang, K., 2010, "Analysis of the Mechanism of Lateral Impact Aortic Isthmus Disruption in Real-Life Motor Vehicle Crashes Using a Computer-Based Finite Element Numeric Model: With Simulation of Prevention Strategies," J. Trauma, **68**(6), pp. 1375–1395.

[5] Yang, K. H., Hu, J., White, N. A., King, A. I., Chou, C. C., and Prasad, P., 2006, "Development of Numerical Models for Injury Biomechanics Research: A Review of 50 Years of Publications in the Stapp Car Crash Conference," Stapp Car Crash J, **50**, pp. 429–490.

[6] Iwamoto, M., Kisanuki, Y., Wantanabe, I., Furusu, K., Miki, K., and Hasegawa, J., 2002, *Development of a Finite Element Model of the Total Human Model for Safety (THUMS) and Application to Injury Reconstruction*, International Research Council on the Biomechanics of Injury, Munich, Germany.

[7] Shigeta, K., Kitagawa, Y., and Yasuki, T., 2009, "Development of Next Generation Human FE Model Capable of Organ Injury Prediction," Enhanced Safety of Vehicle Conference, Stuttgart, Germany, June 15–18, Paper No. 09-0111.

[8] Danelson, K., Bolte, J. H., and Stitzel, J. D., 2011, "Assessing Astronaut Injury Potential From Suit Connectors Using a Human Body Finite Element Model," Aviat. Space Environ. Med., **82**(2), pp. 79–86.

[9] Eppinger, R., Sun, E., Bandak, F., Haffner, M., Khaewpong, N., Maltese, M., Kuppa, S., Nguyen, T., Takhounts, E., Tannous, R., Zhang, A., and Saul, R., 1999, "Development of Improved Injury Criteria for the Assessment of Advanced Automotive Restraint Systems—II," National Highway Traffic Safety Administration, Department of Transportation Report, Docket No. 1999-6407-5.

[10] Kallieris, D., Rizzetti, A., Mattern, R., Jost, S., Priemer, P., and Unger, M., 1997, "Response and Vulnerability of the Upper Arm Through Side Air Bag Deployment," 41st Stapp Car Crash Conference, Lake Buena Vista, FL, SAE Technical Paper No. 973323, pp. 101–110.

[11] Kemper, A. R., Stitzel, J. D., Mcnally, C., Gabler, H. C., and Duma, S. M., 2009, "Biomechanical Response of the Human Clavicle: The Effects of Loading Direction on Bending Properties," J. Appl. Biomech., **25**(2), pp. 165–174.

[12] SAE, 2007, "Surface Vehicle Recommended Practice, Instrumentation for Impact Test—Part 1—Electronic Instrumentation," SAE International, SAE Paper No. J211.

[13] Lau, I. V., and Viano, D. C., 1986, "The Viscous Criterion- Basis and Applications of an Injury Severity Index for Soft Tissues," 30th Stapp Car Crash Conference, San Diego, CA, Oct., SAE Paper No. 861882, pp. 123–142.

[14] Sprague, M. A., and Geers, T. L., 2010, "A Residual-Potential Boundary for Time-Dependent, Infinite-Domain Problems in Computational Acoustics," J. Acoust. Soc. Am., **127**(2), pp. 675–682.

[15] U.S. Department of Transportation, Federal Motor Vehicle Safety Standard 208.

[16] Kemper, A. R., Mcnally, C., Kennedy, E. A., Manoogian, S. J., Rath, A. L., Ng, T. P., Stitzel, J. D., Smith, E. P., Duma, S. M., and Matsuoka, F., 2005, "Material Properties of Human Rib Cortical Bone From Dynamic Tension Coupon Testing," Stapp Car Crash J., **49**, pp. 199–230.

[17] Kemper, A. R., Mcnally, C., Pullins, C. A., Freeman, L. J., Duma, S. M., and Rouhana, S. M., 2007, "The Biomechanics of Human Ribs: Material and Structural Properties From Dynamic Tension and Bending Tests," Stapp Car Crash J., **51**, pp. 235–273.

[18] Stitzel, J. D., Cormier, J. M., Barretta, J. T., Kennedy, E. A., Smith, E. P., Rath, A. L., Duma, S. M., and Matsuoka, F., 2003, "Defining Regional Variation in the Material Properties of Human Rib Cortical Bone and Its Effect on Fracture Prediction," Stapp Car Crash J., **47**, pp. 243–265.

[19] LeBlanc, A. D., Spector, E. R., Evans, H. J., and Sibonga, J. D., 2007, "Skeletal Responses to Space Flight and the Bed Rest Analog: A Review," J. Musculoskelet. Neuronal Interact., **7**(1), pp. 33–47.